# Mapping the operating performance of a novel internally circulating fluidized bed reactor applied to chemical looping combustion

Mogahid Osman[1], Abdelghafour Zaabout[2], Schalk Cloete[2], Shahriar Amini[1,2*]
[1]Norwegian University of Science and Technology, Department of Energy and Process Engineering
[2]SINTEF Industry, Process Technology Department
Trondheim, Norway

## Abstract

Chemical looping combustion is a promising technology for minimizing the energy penalty of $CO_2$ capture. To accelerate the scale-up and commercialization of this technology for pressurized operation, the internally circulating reactor (ICR) was recently proposed. ICR integrates the two reactors, cyclones, loop seals and solids transport lines of the conventional chemical looping configuration into a single unit that simplifies design and operation. This work reports the ICR operating performance over a range of operating parameters applied to chemical looping combustion (CLC). The concept proved relatively simple to operate, allowing the oxygen-carrier circulation rate to be controlled over a wide range by varying the bed loading and the air reactor feed rate. Fully autothermal CLC operation was demonstrated as an illustration of the ease of ICR operation. Gas leakage between the two reactor chambers decreased strongly with decreasing solids loading, resulting in $CO_2$ capture and purity up to 94% for the lowest bed loading. The data showed that significant room for further optimization of the solids transport ports in the reactor exists, which will further increase the $CO_2$ separation performance. These results demonstrate the promise of ICR concept and provide valuable insights for the design of larger-scale units in future work.

**Keywords**: Chemical Looping Combustion; Internally Circulating Reactor; $CO_2$ Capture; Fluidized bed Reactor; Oxygen Carrier

[*]Corresponding author: Dr. Shahriar Amini, SINTEF Industry, S.P. Andersens vei 15 B, 7031, Trondheim, Norway, Phone: +47 46639721, Email: shahriar.amini@sintef.no

**Nomenclature**

| | |
|---|---|
| AR | Air reactor |
| CLC | Chemical looping combustion |
| CLOU | Chemical looping oxygen uncoupling |
| FR | Fuel reactor |
| ICR | Internally circulating reactor |
| OC | Oxygen carrier |
| | |
| $F_{i_{CO}}$ | CO molar flowrate at FR inlet (mol/min) |
| $F_{o_{CO}}$ | CO molar flowrate at FR outlet (mol/min) |
| $F_{AR,o_{CO_2}}$ | $CO_2$ flowrate at AR outlet (Nl/min) |
| $F_{FR,i_{CO}}$ | CO flowrate at FR inlet (Nl/min) |
| $F_{FR,o_{CO_2}}$ | $CO_2$ flowrate at FR outlet (Nl/min) |
| $F_{FR,o_{tot}}$ | Total FR outlet flowrate (Nl/min) |
| $F_{FR,i_{N_2}}$ | $N_2$ flowrate at FR inlet (Nl/min) |
| $F_{O_{2,AR,in}}$ | Inlet molar flowrate of oxygen to the AR |
| $m_{OC}$ | Actual mass of the OC in its partially oxidized state (g) |
| $m_{OC_{ox}}$ | Mass of the fully oxidized OC (g) |
| $m_{O_2}$ | Mass of $O_2$ consumed during the re-oxidation test (g) |
| $\dot{m}_s$ | Solids circulation rate (g/s) |
| $M_{O_2}$ | Molecular weight of oxygen |
| $R_o$ | Oxygen transport capacity of the OC |
| $X_{s,FR}$ | Solids conversion in FR |
| $X_{s,AR}$ | Solids conversion in AR |
| $x_{O_2}$ | Oxygen conversion at outlet of AR |
| $\Delta X_s$ | Solids conversion difference between AR and FR |
| $\gamma_{CO}$ | Conversion of CO, % |

## 1. Introduction

The global energy demand projected to rise by 25% by 2040 (according to the 2018 Energy Outlook issued by the international energy agency IEA [1]) and hence fossil fuels will most likely remain the backbone of the global energy system for the coming decades [1]. Carbon capture and storage CCS has the potential to reduce $CO_2$ emissions from fossil fuel utilization in order to fulfil the ambitions of Paris agreement in limiting future temperature increases to 2°C [1]. Among the different alternative technologies for CCS, chemical looping combustion (CLC) is viewed as a promising technology that allows generation of cleaner energy from fossil fuel with inherent $CO_2$ capture and high overall power plant efficiency [2]. The CLC system avoids direct air and fuel contact by utilizing an oxygen-carrier martial circulated between two

interconnected reactors, namely the air reactor and the fuel reactor [3,4]. In the fuel reactor, the fuel reacts with the metal oxide to form $CO_2$ and $H_2O$, from which a pure $CO_2$ stream can easily be produced by condensing the water. In the air reactor, the reduced metal is oxidized and heated by the highly exothermic reaction before being transferred to the fuel reactor for continuous cyclic operation. The large stream of hot $CO_2$-free gas from the air reactor can drive a power cycle.

To achieve competitive power plant efficiencies with gaseous fuels, pressurized operation of the CLC process is essential to enable integration with a combined power cycle. A thermodynamic assessment has shown that a pressurized CLC (PCLC) system integrated with a natural gas combined cycle (NGCC) resulted in a power efficiency of 52-55% (LHV), which is about 3-5 %-points more efficient than NGCC with post-combustion $CO_2$ capture [5,6]. Nevertheless, the CLC process has mostly been studied at atmospheric pressure operation, given that the dual circulating fluidized-bed reactor is the most widely used reactor configuration for CLC system. Extensive investigations using this configuration had been conducted using lab [7–9] and pilot scales [10,11]. The conventional dual-circulating fluidized-bed configuration combined two interconnected reactors and a gas-solid separation system (loop seals and cyclones) to avoid gas leakage between the fuel and air reactors. To achieve a pressurized CLC, this configuration requires a separate pressure shell for each of these interconnected components and careful management of the pressure in each unit to ensure reliable solids circulation. Thus far, gas-fueled CLC scale-up has been slow, even though almost all studies were done under atmospheric pressure [2]. Accelerating this scale-up process while adding the significant complexity of pressurized operation requires a different approach.

Alternative reactor configurations have been proposed by many researchers to avoid external solids circulation and ease pressurized operation. The gas-switching concept is one of such reactor configurations, where alternate streams of air and fuel are introduced to one fluidized-

bed reactor that contains the oxygen carrier material [12,13]. This concept greatly simplifies the reactor design and scale-up, but a coordinated cluster of reactors is required to achieve steady operation. Other reactor concepts proposed in the literature are the moving bed [14,15] and rotating bed reactor [16,17].

However, the circulating fluidized-bed configuration remains an attractive option considering its steady-state nature, high gas throughput rates and excellent intra-particle and interphase heat and mass transfer. It is possible, however, that the solids circulation mechanism will have to be simplified considerably for this reactor configuration to achieve successful scale-up and eventual commercialization for pressurized CLC. For this reason, this paper investigates the recently proposed internally circulating fluidized-bed reactor (ICR) where the loop seals involved in the conventional configuration are replaced by simple ports between two chambers in a single vessel, with a freeboard on the top replacing the cyclones [18,19]. The ICR concept (as shown in Fig. 1) was especially designed to simplify scale up of the conventional dual circulating fluidized bed chemical looping configuration for pressurized operation.

In ICR, the functionality of two reactors, two cyclones and two loop seals are combined into a single unit, which can be designed and operated in a single pressure shell. The ICR operates in a similar way as the conventional interconnected CLC reactor configuration; where gaseous fuel and air are fed at different velocities to separate chambers containing a bed of oxygen carrier initially placed in the reactor. The high velocity gas feed in the fast chamber transports solids to the freeboard. The decelerated solids in the freeboard (due to the larger chamber area) fall into the upper port to circulate to the second chamber operating at low velocity (the slow chamber). Accumulation of solids in this chamber leads to static pressure build-up, forcing the solids to circulate back to the fast chamber through the port at the bottom.

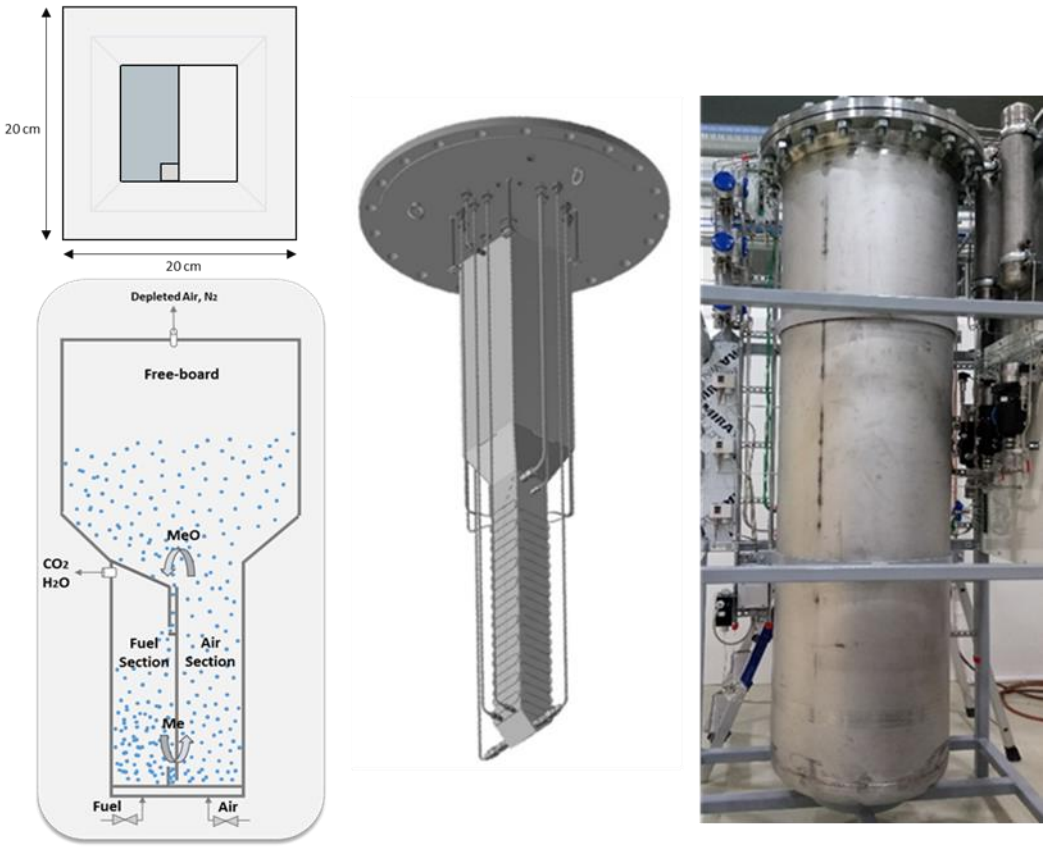


Fig. 1. From left to right; a simplified scheme of the ICR design showing top view and front side view of ICR, CAD drawing of the ICR unit, and the ICR unit under operation inside the shell (Modified from Osman et al. [19]).

The compactness of the ICR concept comes at the expense of gas leakage, which takes place between the two reactor chambers through the connecting ports. A hydrodynamic investigation on a pseudo-2D cold-flow ICR unit has revealed that stable solids circulation and minimum gas leakage could be achieved over a wide range of operating conditions [18], and they can be controlled by adjusting the ratio of the gas velocities in the air and fuel champers, in addition to the solids loading in the reactor. This conclusion was confirmed by reactive multiphase flow modelling of a large-scale ICR unit (100 $MW_{th}$) reactor [20]. In light of the promising results from the hydrodynamic study and the reactive simulations, the ICR unit shown in **Error! Reference source not found.** has been constructed and commissioned to operate under fully reactive high temperature pressurized conditions. The unit had been successfully demonstrated for chemical looping methane reforming to syngas under atmospheric operation [19].

The aim of this study is to gain a full understanding on the process parameters that affect the ICR performance in terms of solids circulation rate, gas leakage between the chambers and fuel conversion under atmospheric conditions. A comprehensive experimental campaign has been conducted with various solids loadings and fluidization velocities in the two reactor chambers. These experiments were completed under chemical looping combustion mode using a $CaMnO_{3-\delta}$-based oxygen carrier and CO as a fuel. To isolate the effect of reaction kinetics, all experiments were completed at nearly constant operating temperature of ~840°C at which high conversion of CO was achieved over $CaMnO_{3-\delta}$-based oxygen carrier [21]. The campaign was carried out at atmospheric pressure to minimize the complexity and cost of carrying out the large number of experiments reported in this study. Accordingly, an operating window maximizing the overall reactor performance was defined for future pressurized operation and further scale-up.

## 2. Methodology

### 2.1. ICR unit

The ICR system consists of a single reactor vessel with partitions creating two interconnected chambers with two connected ports at the top and the bottom, as well as a freeboard region for minimizing particle elutriation (Fig. 1). The chambers have equal cross-sectional areas ($0.05\times0.1$ $m^2$) and heights of 70 cm. One of the chamber (the air reactor AR) is connected to an expanding freeboard for decelerating the gas so that solids can fall into the top port for transport to the another chamber (the fuel reactor FR). The mechanisms by which solids circulation between the chambers occurs is as follows: by feeding the gas at a sufficiently high velocity into the AR, the solid particles will transport to the freeboard where the gas velocity decelerates causing the solids to fall down into the FR through the top connecting port. The accumulation of solids in the FR, which is operated with a lower gas velocity, will create a static pressure build up, forcing the solids to circulate back to the AR through the connecting

port at the bottom. It should be noted that the freeboard was made large enough to enable the flexibility of running a wide range of operating conditions needed in this research phase of the concept, while maintaining minimal solids elutriation. Further refinement of the design of the different components of the reactor could be implemented when the process behavior is well understood.

The gas feed to each reactor chamber is introduced using a perforated cylindrical tube at the bottom of each chamber. The ports connecting the two chambers are L-type connection ports, which were adopted instead of a simple orifice to create conditions with solids flowing close to maximum packing. Such a flow condition creates a physical plug that minimizes undesired gas leakage through the port. The top port connects the freeboard and the FR at the corner opposite to the FR gas outlet as shown in the top view of ICR in Fig. 1. More details about the unit design and specifications can be found in a previous study where this ICR system was used for chemical looping reforming of methane using a NiO-based oxygen carrier [19].

Fig. 2. gives the layout of the unit and its different auxiliary components. In addition to the reactor, the experimental setup includes heat exchangers placed on the outlet of each chamber for cooling down the exhaust streams before being sent to the atmosphere. Low temperature filters (5 μm pore size) installed after the coolers were used to collect elutriated fine particles. The dry gas composition (sampled after the filters) was measured using an analyzer (MCA 100 Syn-P from ETG Risorse e Tecnologia). Additional devices were used for controlling and monitoring reactor operation and for safety measures, including mass flow controllers for gas feed, thermocouples, pressure sensors and valves.

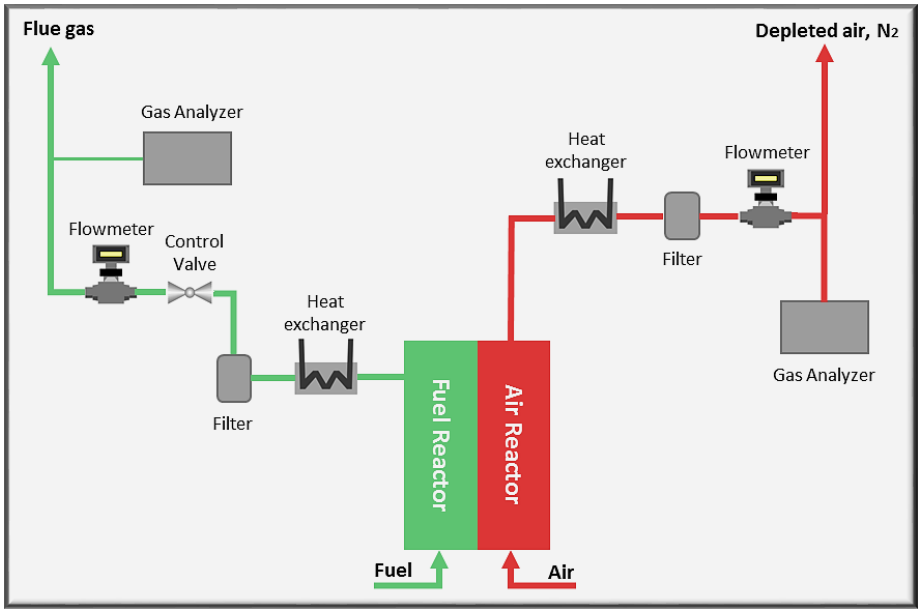

Fig. 2. Simplified illustration of the ICR auxiliary components.

## 2.2. Oxygen carrier

In this study, an oxygen carrier (OC) based on calcium manganite with a perovskite structure was used. The oxygen carrier has a nominal composition of ($CaMn_{0.775}Ti_{0.125}Mg_{0.1}O_{3-\delta}$), and was manufactured by VITO (Flemish institute for technological research) through the spray-drying method. Ti and Mg were added to the structure to improve fuel conversion, fluidization properties and mechanical stability [22]. The δ-factor describes the oxygen deficiency in the perovskite structure, where $O_2$ is released in the fuel reactor (FR) in a low $O_2$ partial pressure environment leading to increased oxygen deficiency, while δ decreases in the air reactor (AR) due to the $O_2$ rich environment leading to oxygen uptake [22–24]. Zaabout et al. [21] calculated the oxygen carrying capacity of this OC as 2.92% at 810°C while higher values were reported at operating temperatures of 950°C showing the high sensitivity to temperature of the CLOU effect of this oxygen carrier [24]. The physical properties of this OC are presented in Table 1. This OC was selected as it showed great promise for CLC application due to its high chemical performance and stability, in addition to the low attrition rate shown in prolonged lab and pilot scale experiments [22,25]. It should however be emphasized that the selection of an optimal oxygen carrier is out of the scope of this study; the main aim is to demonstrate the experimental

feasibility of the ICR concept applied to CLC and map out its performance in terms of solids circulation rate, and $CO_2$ purity and capture efficiency.

**Table 1 – Properties of the $CaMn_{0.775}Ti_{0.125}Mg_{0.1}O_{3-\delta}$ oxygen carrier used in this study**

| Parameter | Value |
|---|---|
| Bulk density (kg/m$^3$) | 1600 |
| Particle size distribution in μm (D10; D50; D90) | 94.2; 134.2; 187.6 |
| Sintering temperature (°C) | 1350 |
| Crushing strength (N) | 2.44 |
| Minimum fluidization velocity at operating conditions for AR (m/s) | 0.013 |
| Minimum fluidization velocity at operating conditions for FR (m/s) | 0.014 |
| Terminal velocity at operating conditions for AR (m/s) | 0.59 |

### 2.3. Experimental procedure

CO was used as fuel in all experiments conducted in this study due to its good reactivity and simple reaction mechanism with the oxygen carrier, keeping the focus of the study on the separation performance and the solids circulation characteristics of the ICR. The fuel was diluted with $N_2$ in most cases to control the heat generation in the system so that all experiments could be carried out at similar temperatures while maintaining the fluidization velocity in the fuel reactor high enough to achieve enough bed expansion for the solids to circulate back to the air chamber through the bottom port. Additionally, this prevents full OC reduction in the fuel reactor, thus minimizing the risk of carbon deposition and large fuel slip.

The solids inventory in the unit was varied as 1.5, 2.5, and 3.5 kg, corresponding to 9.4, 15.6, and 21.8 cm static-bed height, respectively. A total of 16 experimental cases was conducted in this study varying the solids inventory, AR flowrate and FR flowrate (Table 2). The flowrate in the FR was varied from 7 to 15 Nl/min and the flowrate in the AR from 30 to 110 Nl/min. At these conditions, bubbling and fast fluidization regimes were established in the FR and AR, respectively. Each case was designed to elucidate the effect of one parameter while maintaining

the others constant. For instance, cases 1, 5 and 6 were designed to investigate the effect of FR flowrate while keeping the AR flowrate and solids inventory constant.

The reactor was electrically heated to 700°C before feeding air and fuel for pushing the temperature up to the target reaction temperature. During the reactive CLC experiments, this target FR bed temperature was kept constant at 840°C for all the cases; hence, the power of the heater was adjusted between 0 to 100% depending on the operating conditions. For autothermal operation, the heater power was set to 0% so that the system temperature is maintained solely through the redox reactions taking place in the CLC process. All experiments were carried out at atmospheric pressure and the experimental results from each case were averaged over at least 30 minutes of steady state operation. Table 3 summarizes the main operating conditions investigated in the current study.

**Table 2 - Experimental cases investigated in this study**

| **Experimental cases** | **Solids Inventory (kg)** | **Flowrate (Nl/min)** | | | |
|---|---|---|---|---|---|
| | | **AR** | **FR** | | |
| | | air | CO | $N_2$ | Total |
| 1 | 1.5 | 50 | 5 | 5 | 10 |
| 2 | | 70 | | | |
| 3 | | 90 | | | |
| 4 | | 110 | | | |
| 5 | | 50 | | 2 | 7 |
| 6 | | 50 | | 10 | 15 |
| 7 | | 60 | 10 | 0 | 10 |
| 8 | | 70 | | | |
| 9 | 2.5 | 30 | 5 | 5 | 10 |
| 10 | | 50 | | | |
| 11 | | 70 | | | |
| 12 | | 50 | | 2 | 7 |
| 13 | 3.5 | 30 | 5 | 2 | 7 |
| 14 | | 40 | | | |
| 15 | | 50 | | | |
| 16 | | 70 | | | |

**Table 3 - The operating conditions investigated in this study**

| Parameter | Value |
|---|---|
| FR bed temperature (°C) | 840 |
| Pressure (bara) | 1.0 |
| Solids inventory (kg) | 1.5, 2.5, 3.5 |
| Bed height (cm) | 9.4, 15.6, 21.8 |
| Fluidization velocity in AR (m/s) | 0.40 - 1.34 |
| Fluidization velocity in FR (m/s) | 0.09 - 0.20 |
| Volumetric flowrate in AR (Nl/min) | 30 - 110 |
| Volumetric flowrate in FR (Nl/min) | 7 - 15 |
| Thermal power of the fuel input | 1 to 2.1 kW |

## 2.4. Data evaluation

### 2.4.1. Fuel conversion

Reactivity of CO with the OC was expressed by $\gamma_{CO}$, the conversion of CO, which is defined as in Eq. (1):

$$\gamma_{CO} = \frac{F_{i_{CO}} - F_{o_{CO}}}{F_{i_{CO}}} \times 100 \quad (1)$$

### 2.4.2. $CO_2$ capture efficiency and purity

Gas leakage between the FR and AR is undesirable because it lowers $CO_2$ capture efficiency and purity. The $CO_2$ capture efficiency can be calculated from the amount of $CO_2$ exiting at the AR outlet according to Eq. (2). Similarly, $CO_2$ purity can be calculated as the percentage of the measured impurities in the $CO_2$ stream at FR outlet (Eq. (3)). Note that the $N_2$ diluting the fuel for the purpose of achieving consistent reactor performance over all the experiments in Table 2**Error! Reference source not found.** is subtracted from the total FR outlet flowrate in the denominator of Eq. (3).

$$\mathrm{CO_2\ capture\ effiency} = \left(1 - \frac{F_{AR,o_{CO_2}}}{F_{FR,i_{CO}}}\right) \times 100 \quad (2)$$

$$\mathrm{CO_2\ purity} = \left(\frac{F_{FR,o_{CO_2}}}{F_{FR,o_{tot}} - F_{FR,i_{N_2}}}\right) \times 100 \quad (3)$$

### 2.4.3. Solids circulation rate

The solids circulation rate is a critical operating variable for the CLC process. Solids circulation between FR and AR is required to transfer oxygen and heat between the two reactors in order to fulfil the mass and heat balance of the system. Estimating the solids circulation rate in a hot ICR system is a challenging task because no direct measurement technique is possible. An indirect approach was adopted in this study, by considering the correlation between the solids circulation rate with the solids conversion difference between the AR and the FR. By re-oxidation of the OC after a steady state CLC experiment, it is possible to estimate the degree of reduction/oxidation of the particles placed in the reactor from the amount of the $O_2$ consumed. Hence the average solids conversion difference between the AR and the FR in the steady state operation can be estimated, which is directly linked to the magnitude of the solids circulation rate during the CLC process. This methodology has been proposed by many CLC studies carried out in a circulating fluidize-bed reactor [3,26–32].

The following procedure was used for the re-oxidation test in the current study, after at least one hour of steady state CLC operation. Fuel feed was replaced with $N_2$ in the FR, while air was kept in the AR. During this experiment, the $O_2$ measurement from the AR outlet provides the $O_2$ consumption by the reduced OC in the reactor. Fig. 3**Error! Reference source not found.** and Fig. 4**Error! Reference source not found.** show an example of the AR oxygen profile during the re-oxidation test for selected cases. In these cases, the re-oxidation tests was carried out using the same flowrates in AR and FR (50 and 10 Nl/min in the AR and FR,

respectively) after steady state operations completed with varying the FR feed at constant AR feed (Fig. 3) and varying the AR feed at constant FR feed (Fig. 4). Fig. 3. reveals that the O2 consumption was insensitive to the FR feed, whereas Fig. 4**Error! Reference source not found.** shows a clear effect of the AR feed. This means that the FR feed rate had no effect on the solids circulation rate, but the AR feed rate had a significant effect.

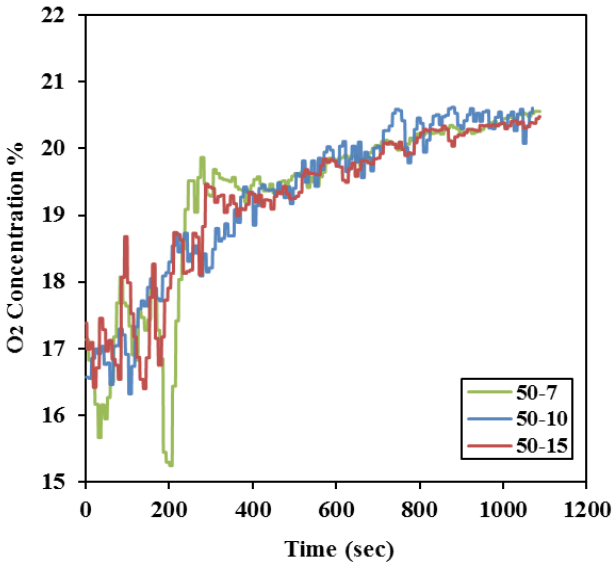


Fig. 3. Transient oxygen concentration at the AR outlet during the re-oxidation test for three CLC cases. The gas flowrate in AR was maintained at 50 Nl/min while the FR flowrate was varied between 7, 10, 15 Nl/min. A1.5 kg solids inventory was used.

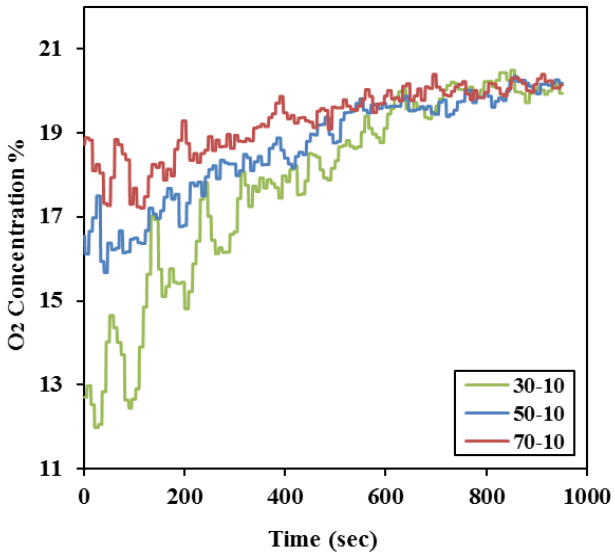


Fig. 4. Transient oxygen concentration at the AR outlet during the re-oxidation test for three CLC cases. The gas flowrate in FR was maintained at 10 Nl/min while the AR flowrate was varied between 30, 50, 70 Nl/min. A 2.5 kg solids inventory was used.

The total $O_2$ consumption $\left(m_{O_2}\right)$ is calculated using the $O_2$ profiles of the re-oxidation tests, which is used for calculating the solids conversion difference as follows:

$$\Delta X_s = X_{s,AR} - X_{s,FR} \tag{4}$$

$$X_s = \frac{m_{OC} - m_{OC_{ox}}(1 - R_o)}{m_{OC_{ox}} R_o} \tag{5}$$

$$m_{OC} = m_{OC_{ox}} - m_{O_2} \tag{6}$$

Two assumptions were considered to estimate the solids conversion difference:

1) The OC was fully oxidized in the AR ($X_{s,AR} = 1$), because air was supplied to the AR in excess. This implies that the $O_2$ consumption during the re-oxidation test was only from the OC in the FR at the start of the test.
2) The mass of the OC was equally distributed between the FR and the AR during the CLC operation. This assumption was considered due to the absence of accurate measurement technique to estimate the actual amount of solids placed in each chamber during the CLC operation.

By combining Eqs. (4), (5) and (6) under the two assumptions given above, the solids conversion difference can be calculated. With the estimate of the solids conversion difference, the solids circulation rate can be calculated using the oxygen balance in the AR: the oxygen consumed in the AR is equal to the oxygen taken by the OC in the AR as in Eq. (7):

$$F_{O_{2,AR,in}} x_{O_2} M_{O_2} = \dot{m}_s R_o \Delta X_s \tag{8}$$

The calculated solids circulation rate should only be considered as a rough estimation, given the considered assumptions.

### 2.4.4. Solids elutriation

In the current study, an oxygen carrier with high stability and low attrition rate was used based on previous prolonged lab and pilot scale experiments [8,9]. Particle elutriation in the current study is therefore mainly due to hydrodynamics in the bed, which will limit the maximum achievable gas feed rates and bed loading. The procedure for estimating solids elutriation was based on collecting the solids found on the filters and the coolers after each experimental case, which corresponds to around 1 hour of a steady state CLC operation. The collected solids were then weighted and sieved. This approach reveals the effect of AR flowrate, FR flowrate and solids inventory on the solids elutriation rate.

## 2.5. Scope of the study

There are two main categories of parameters that affect the performance of a given ICR when applied to the CLC process; the oxygen carrier properties and the operating conditions. Among the different parameters, the focus in this study was on the role played by the solids inventory and the fluidization velocity in AR and FR on various ICR performance measures, which include $CO_2$ capture efficiency and purity, fuel conversion, solids circulation rate and solids elutriation rate. The aim is to find an operating window that maximizes the overall reactor performance by achieving high fuel conversion and $CO_2$ separation performance and low solids elutriation. Based on this knowledge, future pressurized operation will be carried out using the best-defined operating conditions.

## 3. Results and Discussion

The results will be presented and discussed in three parts: 1) Effect of AR flowrate and solids inventory, 2) Effect of FR flowrate, and 3) Autothermal CLC operation. Four performance measures will be evaluated: 1) Fuel conversion, 2) Solids circulation rates, 3) $CO_2$ capture

efficiency and purity, and 4) Solids elutriation. Table 4 summarizes the main results of all the CLC experimental campaigns which will be discussed in the following sections.

An example of the concentration of the outlet gas from the FR and AR for a typical CLC operation is shown in Fig. 5. It could be seen that steady state operation was achieved for a prolonged period resulting in relatively constant $CO_2$ production in the FR and stable consumption of $O_2$ in the AR. This demonstrates the ability of the ICR reactor in establishing stable solids circulation between the chambers, transferring oxygen from AR to oxidize the fuel fed to the FR. Traces of $CO_2$ was measured in the AR outlet indicating presence of gas leakage between the chambers. It should be emphasized that the high oxygen excess in the AR, as shown in Fig. 5 and Table 4 for the other cases, is due to the use of a limited fuel input in this study to avoid excessive temperature rise in the AR in the cases with lower air flowrates (less air to remove heat from the system). Such a temperature rise had to be prevented to ensure that all cases were operated at a constant temperature. However, in a real CLC process the air to fuel ratio should be adjusted to maximize the system performance.

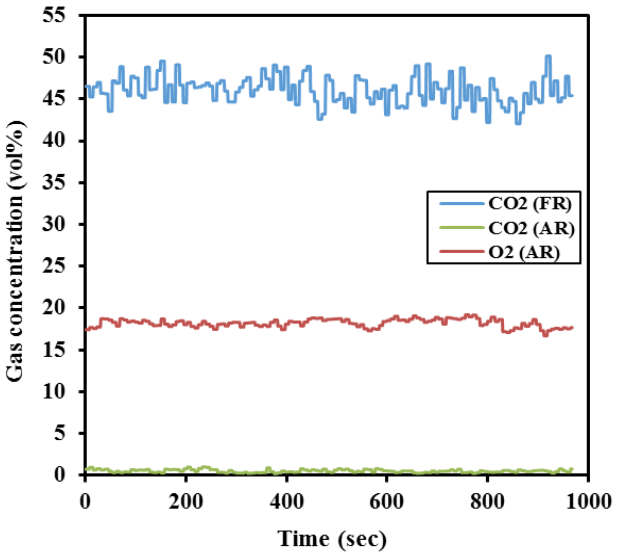


Fig. 5. Gas product distribution obtained at the outlet of FR and AR during CLC tests for case 2 in Table 4.

**Table 4 - Summary of the main results of the CLC experimental campaigns**

| Experimental cases | Solids Inventory (kg) | Flowrate Nl/min | | | Products Concentration (vol%) | | | | | | CO Conversion % | $CO_2$ Capture Efficiency % | $CO_2$ Purity % | Solids circulation rate (g/s) | Solids elutriation (g) |
|---|---|---|---|---|---|---|---|---|---|---|---|---|---|---|---|
| | | AR | FR | | FR | | | | AR | | | | | | |
| | | air | CO | $N_2$ | CO | $CO_2$ | $O_2$ | $N_2$ | $CO_2$ | $O_2$ | | | | | |
| 1 | **1.5** | 50 | 5 | 5 | 0.90 | 45.30 | 0.29 | 53.51 | 0.84 | 16.99 | 98.2 | 92.0 | 92.4 | 2.8 | 6 |
| 2 | | 70 | | | 0.52 | 46.05 | 0.31 | 53.12 | 0.51 | 18.20 | 99.0 | 93.1 | 93.1 | 3.6 | 8 |
| 3 | | 90 | | | 0.31 | 46.47 | 0.38 | 52.83 | 0.38 | 18.85 | 99.4 | 93.3 | 93.6 | 6.1 | 15 |
| 4 | | 110 | | | 0.00 | 45.58 | 0.60 | 53.82 | 0.35 | 18.98 | 100.0 | 92.4 | 91.2 | 7.0 | 54 |
| 5 | | 50 | | 2 | 0.15 | 65.09 | 1.12 | 33.65 | 0.92 | 17.02 | 99.8 | 91.2 | 91.3 | 2.7 | - |
| 6 | | 50 | | 10 | 1.21 | 30.06 | 0.15 | 68.58 | 0.60 | 17.04 | 96.4 | 94.2 | 93.8 | 2.7 | 11 |
| 7 | | 60 | 10 | 0 | 2.92 | 89.25 | 0.56 | 7.27 | 1.32 | 14.16 | 97.1 | 92.7 | 92.2 | - | - |
| 8 | | 70 | | | 3.08 | 89.18 | 0.58 | 7.17 | 1.21 | 15.23 | 96.9 | 92.2 | 92.3 | - | - |
| 9 | **2.5** | 30 | 5 | 5 | 0.3 | 43.8 | 0.2 | 55.7 | 2.7 | 13.3 | 99.4 | 85.0 | 87.5 | 2.6 | 6 |
| 10 | | 50 | | | 0.0 | 41.6 | 0.4 | 58.1 | 1.9 | 17.0 | 100.0 | 81.5 | 83.1 | 4.3 | 14 |
| 11 | | 70 | | | 0.0 | 41.2 | 0.6 | 58.2 | 1.5 | 18.2 | 100.0 | 79.1 | 82.4 | 6.9 | 25 |
| 12 | | 50 | | 2 | 0.0 | 58.4 | 0.8 | 40.9 | 2.2 | 17.0 | 100.0 | 78.6 | 81.7 | 4.4 | 11 |
| 13 | **3.5** | 30 | 5 | 2 | 0.0 | 53.7 | 0.8 | 45.4 | 4.7 | 13.9 | 100.0 | 73.5 | 75.2 | 4.7 | 7 |
| 14 | | 40 | | | 0.0 | 53.0 | 1.3 | 45.7 | 3.4 | 15.9 | 100.0 | 74.5 | 74.2 | 6.5 | 20 |
| 15 | | 50 | | | 0.0 | 52.6 | 1.3 | 46.1 | 2.7 | 17.0 | 100.0 | 74.2 | 73.7 | 8.1 | 28 |
| 16 | | 70 | | | 0.0 | 51.9 | 2.0 | 46.1 | 2.0 | 18.3 | 100.0 | 73.1 | 72.7 | 10.2 | 44 |

### 3.1. Effect of AR flowrate and solids inventory

In this section, the impact of AR flowrate and solids inventory on ICR performance will be presented and discussed. Cases (1-4, 9-11, and 13-16) were designed to study the effect of the AR flowrates for three different solids inventories. CO flowrate was maintained the same for all cases (5 Nl/min), while the total FR flowrate was lowered for the case with the highest bed loading. Specifically, for the 1.5 and 2.5 kg solids inventory cases, 10 Nl/min was used as a total flow rate, while 7 Nl/min was used for 3.5 kg solids inventory cases to minimize solids elutriation due to large bed expansion.

#### 3.1.1. Solids circulation rate

The solids circulation rate was estimated based on the procedure described in section (2.4.3) by re-oxidation of the OC after a steady state CLC test. Fig. 6 shows the effect of the AR flowrate on the solids circulation rate and the solids conversion difference for the different solids inventories considered in this study. It was observed that the solids circulation rate increases with the AR flowrate and the solids inventory. This result is expected given that the AR flowrate and the solids inventory are the main controlling parameters of solids circulation in the ICR system as observed in our previous study on a pseudo-2D ICR cold flow unit [18]. In this previous study, solids circulation rate was found to be tightly linked to the pressure difference between the FR and AR chambers where a larger pressure difference drives larger quantities of solids to circulate from the FR to the AR [18].

Specifically, a larger AR flowrate and solids inventory result in greater bed expansion in the AR, transporting more solids to the freeboard to gain access to the top port for transport to the FR. The resulting larger accumulation of solids in the FR results in a larger static pressure build-up, the driving force for solids transport through the bottom port. This is also in line with findings in previous studies that reported similar mechanisms controlling solids circulation in

interconnected fluidized bed reactors and confirmed the tight correlation between the solids circulation rate and the two independent parameters which are the AR flowrate and solids inventory [18,27,33–37]. It is also important to emphasize that, in the ICR system, a sufficiently large AR flowrate or solids inventory (or both) is needed for achieving acceptable solids circulation rates. For instance, in the present study the case of the 1.5 kg solids inventory, very little or no solids circulation was observed at AR flowrate below 50 Nl/min.

Fig. 6 also shows that larger solids circulation rates, when the AR flowrate or solids inventory (or both) are increased, decreases the solids conversion difference between the chambers. This result is expected because the amount of oxygen transport required to oxidize the fuel stays constant in all cases due to the constant fuel feed rate. Larger solids circulation rates require a lower degree of conversion to transport oxygen from the AR to the FR at a constant rate.

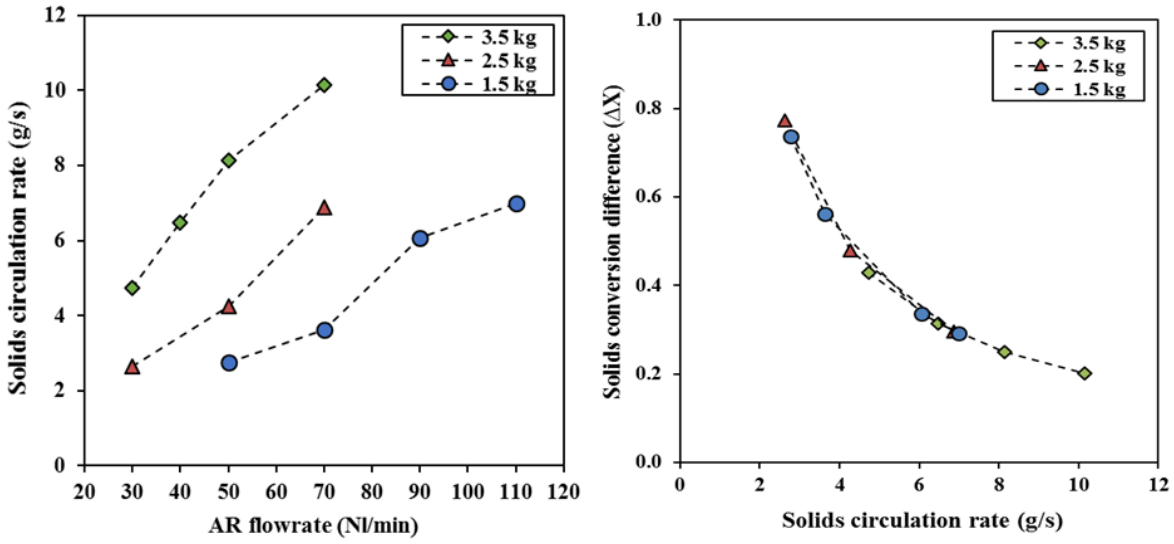


Fig. 6. Solids circulation rate and solids conversion difference with various AR flowrates for different solids inventory, FR flowrate = 7.0 Nl/min (for 3.5 kg solids inventory) and 10 Nl/min (for 1.5, 2.5 kg solids inventory), Cases (1-4, 9-11, and 13-16).

### 3.1.2. Fuel conversion

Fig. 7 shows the effect of the solids circulation rate on CO conversion for the three studied solids inventories. Complete CO conversion is observed for the 3.5 kg solids inventory for all

solids circulation rate, while small CO slippage was detected for the 1.5 kg solids inventory (the poorest achieved CO conversion was 98% that improved with feeding larger AR flowrates). Fuel slippage with the lower solids inventory could be explained either by the lower solids circulation rate or by the shorter bed height. At constant FR flowrate, short bed heights lead to smaller gas residence time in the bed, which reduces the gas-solids contact quality, thus negatively affecting CO conversion. This effect is accentuated in the current ICR setup because the gas is injected using a perforated cylindrical tube in a relatively concentrated manner, imposing significant bubble-to-emulsion mass transfer limitations.

Another explanation for the fuel slippage could be originated from the correlation between the reaction rate and the solids circulation rate. A lower solids circulation rate increases the OC conversion difference between the AR and FR as illustrated in Fig. 6. If the AR oxygen carrier conversion is assumed to be 1 and the highest solids conversion differences approach 0.8 in Fig. 6, the OC conversion in the FR is only about 0.2 (implying it is about 80% reduced). The reaction rate of the reduction reaction decreases significantly at lower OC conversions because less oxidized oxygen carrier is available for reaction, and this could explain the greater fuel slip with higher degrees of solids conversion difference at lower solids circulation rate and the lowest solids loading as observed in Fig. 6 and Fig. 7.

In this case, given the short bed heights and the concentrated fuel injection, the low fuel slippage observed for the cases with low solids circulation is testament to the high reactivity of the OC used in this study. In a larger scale ICR reactor, the greater gas residence time should easily ensure full conversion of the fuel, even at high degrees of OC reduction.

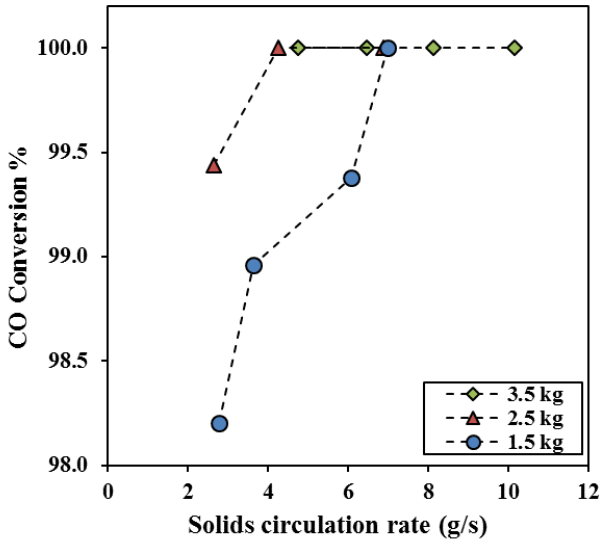


Fig. 7. CO conversion with various solids circulation rate for different solids inventory, FR flowrate = 7.0 Nl/min (for 3.5 kg solids inventory) and 10 Nl/min (for 1.5, 2.5 kg solids inventory), Cases (1-3, 9-11, and 13-16).

### 3.1.3. $CO_2$ capture efficiency and purity

The gas leakage between the two reactor chambers is a critical parameter in ICR performance and should be minimized to maximize $CO_2$ capture efficiency and purity. Gas leakage can be controlled by ensuring that the gas outflow is equivalent to the gas inflow in each chamber. The gas leakage mainly occurs as a result of the gas being dragged with the circulated solids or as a result of pressure-induced flow. If there is a gas leak from the FR to the AR, the $CO_2$ capture efficiency will decrease since part of the combusted gas will leak to the AR where the slipped $CO_2$ is vented to the atmosphere. Gas leakage in the other direction will cause the $CO_2$ stream to be diluted with nitrogen from AR, reducing the $CO_2$ purity.

Fig. 8. shows the calculated $CO_2$ capture efficiency and purity with different solids circulation rates for the various solids inventories studied. One can observe that the solids circulation rate slightly affects the $CO_2$ capture efficiency and purity, while the solids inventory has a much larger effect. Fig. 9. isolates the effect of solids inventory at fixed AR and FR feed rates, showing that the larger solids circulation rates allowed by larger solids inventories comes at the cost of more gas mixing and reduced $CO_2$ separation performance. However, this large

trade-off between solids circulation rate and $CO_2$ separation performance seems to be much smaller when the solids circulation rate is changed by changing the AR flowrate (Fig. 8). Despite the large increase in solids circulation with AR flowrate for all bed loadings (Fig. 6), the $CO_2$ separation performance showed only small sensitivities. In the 1.5 kg bed loading, larger solid circulation rates allowed by higher AR flowrates even slightly improved $CO_2$ capture and purity (Fig. 8).

This implies that there are other factors affecting this leakage phenomenon, which is mostly related to design and hydrodynamic characteristic of the ICR system. As has been stated in section (3.1.1), increasing the solids inventory increases the pressure difference at the bottom of the two chambers, and the pressure drop especially in the FR chamber operating at dense bed conditions. This causes larger resistance for the gas to flow through the bed and enhances the driving force for the gas to leak mostly through the bottom port of ICR. Similar observation was revealed by Latif [33] using a cold model of an internally circulating fluidized-bed gasification system. They attributed the increase of the gas leakage with the solids inventory to the increase of the bed height in the combustor, which in turn increases the resistive force to the up-flowing gas. The study conducted on the pseudo-2D cold flow unit of the ICR system [18] also revealed the same trend of increased gas leakage with increasing the solids inventory, which was correlated to the increase of the pressure difference between the two chambers. The ICR pseudo-2D cold flow system has also revealed development of gas pocket leakage at the bottom port increased size as the solids inventory is increased [18]. Similar behavior should be expected in the hot ICR rig used in the present study that has a similar design as the cold flow unit used in [18].

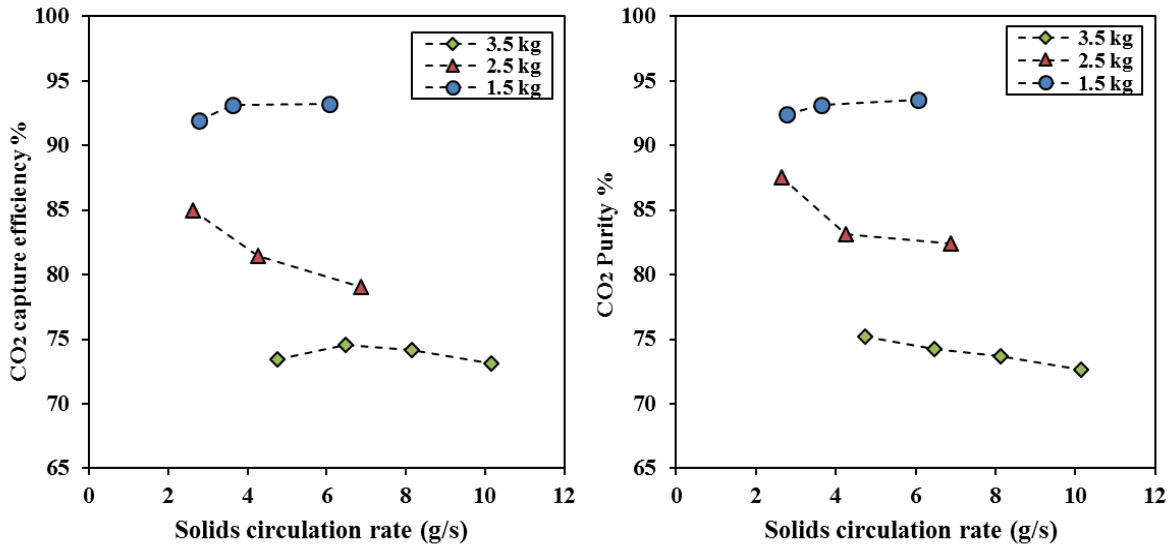


Fig. 8. $CO_2$ capture efficiency and purity % as function of solids circulation rate for different solids inventory, FR flowrate = 7.0 Nl/min (for 3.5 kg solids inventory) and 10 Nl/min (for 1.5, 2.5 kg solids inventory), Cases (1-4, 9-13, and 13-16).

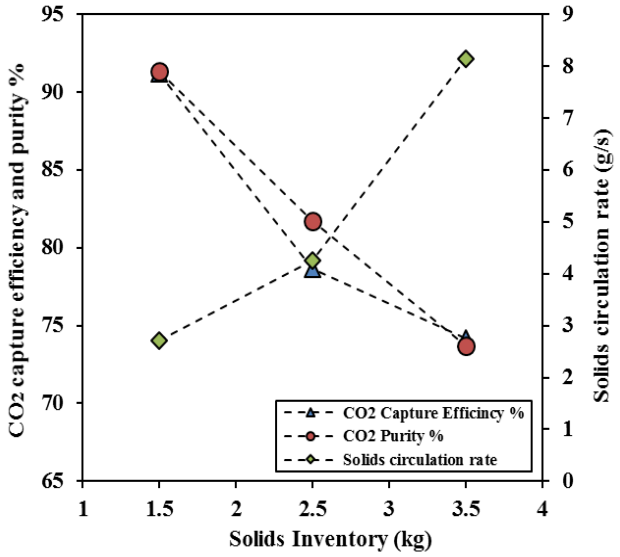


Fig. 9. $CO_2$ capture efficiency and purity and solids circulation rate with various solids inventories, FR flowrate = 7.0 Nl/min, AR flowrate = 50 Nl/min, cases (5, 12 and 15).

In the present ICR setup, the measurements of $O_2$ concentration at the FR outlet (Table 4) allows for additional insight into the gas leakage behavior, specifically whether gas leakage from the AR to the FR occurred through the top or bottom port. $O_2$ in the gas leaking from the AR to the FR through the bottom port will be consumed by reaction with the fuel and oxygen

carrier at the bottom of the FR. On the other hand, $O_2$ leaking from the AR to the FR through the top port will experience minimal or no reaction and can therefore reach the FR outlet.

Fig. 10. illustrates the large difference between the $CO_2$ purity calculated using Eq. (3) and the estimated $CO_2$ purity that would be observed with only gas leakage through the top port using the following equation:

$$CO_2 \text{ purity top port } = \left(1 - \frac{y_{FR,o_{O_2}} / y_{AR,o_{O_2}}}{y_{FR,o_{CO_2}} + y_{FR,o_{O_2}} / y_{AR,o_{O_2}}}\right) \times 100 \qquad (9)$$

In Eq. (9), the ratio of $O_2$ mole fractions at the FR and AR outlets $\left(y_{FR,o_{O_2}} / y_{AR,o_{O_2}}\right)$ represents the estimated mole fraction of all impurities at the FR outlet originating from gas leakage through the top port, assuming that $N_2$ will leak with $O_2$ in the same ratio with which they are present at the AR outlet. It should be noted that this estimation of gas leakage through the top port using $O_2$ mole fraction data is only valid for the cases where fuel conversion was complete (no possibility for $O_2$ slipping through the top port to react with slipped fuel above the bed). For this reason, only the two larger bed loadings are included in Fig. 10.

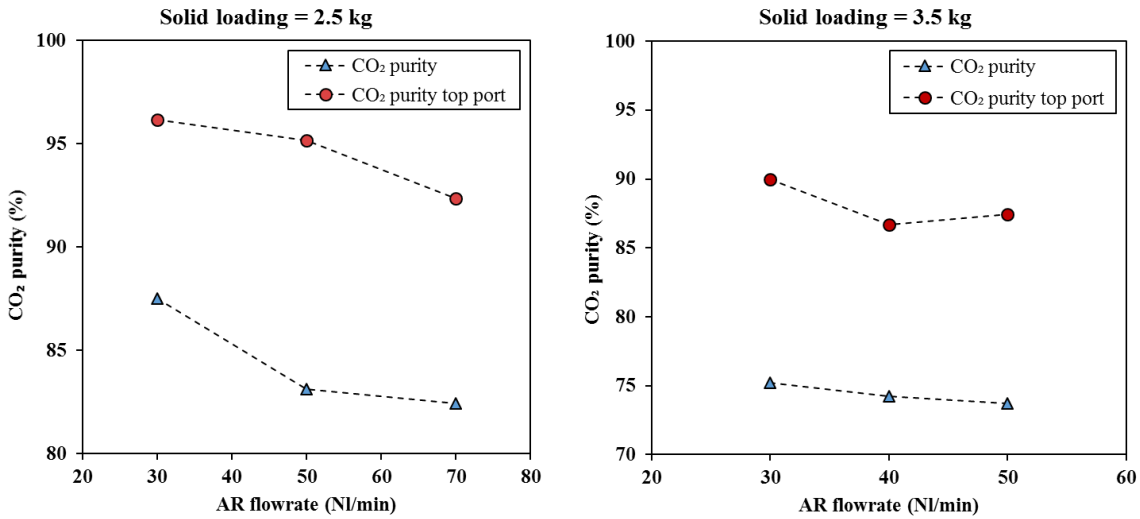


Fig. 10. Comparison of the total $CO_2$ purity to the $CO_2$ purity that would be observed if gas leakage from the AR to the FR occurred only through the top port with the circulation of the OC.

Fig. 10. shows that the $CO_2$ purity originating only from the top port is much better than the total $CO_2$ purity observed in the experiments from both ports. Under ideal ICR operation, all gas leakage from the AR to the FR would occur through the top port with the OC circulation. In this case, however, the data indicates that most gas leakage from AR to FR occurred through the bottom port. The implication of this finding is that regular instances of reverse flow occur through the bottom port, which was also observed for taller beds in the aforementioned cold-flow experiments [18]. This effect is most likely driven by the dynamic nature of pressure fluctuations at the bottom of the two ICR chambers. Although the mean pressure at the bottom of the FR should be higher than the mean pressure at the bottom of the AR, the dynamic fluctuations of both pressure signals frequently create instances where the pressure at the bottom of the AR is higher than at the bottom of the FR, driving gas from the AR into the FR.

The design of the bottom port in ICR systems therefore appears to be very important to attenuate these backflows and minimize the resulting undesired gas leakage. For example, making the bottom port smaller will increase the flow resistance through the port, resulting in a larger solids accumulation in the FR and a larger average overpressure, reducing the likelihood of instantaneous reversals of the pressure gradient. A longer port will also reduce the likelihood that short-lived reversals of the pressure gradient will be able to force gas from the AR into the FR through the bottom port.

Naturally, the extent to which the port can be made smaller and longer is limited by the need to maintain a sufficiently high solids circulation rate to supply oxygen to the reduction reaction taking place in the FR. The present ICR setup was designed with conservatively large ports to ensure that sufficient solids circulation will be possible over a wide range of experimental tests, but future scaled-up ICR units should be designed with the minimum port size at which the required circulation rate can be achieved to minimize gas leakage. Another interesting topic for

future work is the injection of a purge gas into the ports to further increase $CO_2$ capture and purity.

Despite the sub-optimal nature of the bottom port in the present ICR reactor design, good $CO_2$ capture rates and purities can still be achieved for the lowest bed loading in Fig. 9. Future optimizations of the ICR design will significantly improve this performance.

### 3.1.4. Solids elutriation

Following the procedure described in section (2.4.4), the solids elutriation was estimated as the mass of solids found in the filters and the coolers after 1 hour of a steady state CLC operation. The collected particles were mostly fine particles with a particle size below 80 μm. Fig. 11. shows the solids elutriation with different AR flowrates for the various solids inventories studied. As expected, increasing AR flowrate increases the solids elutriation for all cases, and higher solids elutriation was observed with higher solids inventory. Case-4 in Table 4 shows that feeding 110 Nl/min to the AR results in the highest solids elutriation of 54 g/hr, which indicates that the fluidization velocity in this case was too high to allow the freeboard to decelerate the solids to prevent excessive elutriation. The resulted solids elutriation rate using ICR system is well within the tolerable limit for CLC process and expected to be improved further for long operation period using the current OC. Furthermore, the elutriation could further be minimized with a better design of the ICR reactor.

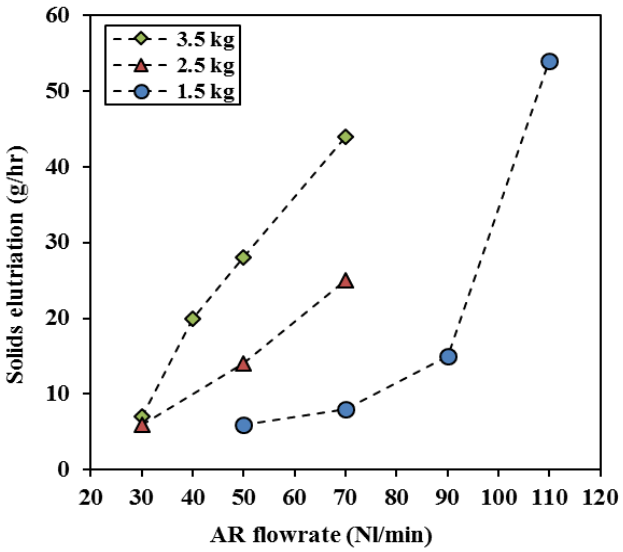


Fig. 11. Solids elutriation with various AR flowrates for different solids inventory, FR flowrate = 7.0 Nl/min for 3.5 kg solids inventory and 10 Nl/min for 1.5, 2.5 kg solids inventory, Cases (1-4, 9-13, and 13-16).

### 3.2. Effect of FR flowrate

To investigate the effect of FR flowrate on ICR performance, experiments were performed with the same AR flowrate (50 Nl/min), solids inventory (1.5 kg) and CO flowrate (5 Nl/min) while varying the total FR flowrate (7, 10, and 15 Nl/min) by altering the amount of $N_2$ dilution to the FR. The three FR flowrates revealed the same solids circulation rate (Table 4), indicating that the solids circulation rate is independent of the FR flowrate. However, increasing the total FR flowrates reduces the CO conversion and increases $CO_2$ capture efficiency and purity as it can be seen in Fig. 12. The reduction of CO conversion is expected since higher gas flowrate lowers the gas residence time in the FR. Also, the reduction of CO partial pressure from increasing $N_2$ dilution contributes to reduce the CO conversion.

The improvement in $CO_2$ capture efficiency and purity with the FR flowrate could be the result improved bed hydrodynamics that moves towards the turbulent regime at higher feed rates, resulting in smoother fluidization behavior with lower pressure fluctuations, thus leading to lower gas leakage between the chambers. In addition, greater expansion of the bed in the FR will increase the mean pressure at the top of the bottom port, reducing the likelihood of

backflow leakage from the AR to the FR. This combination of a higher mean pressure difference and a lower degree of pressure fluctuations cause better gas leakage performance through the bottom port.

Increasing the FR flowrates also increases the solids elutriation (Table 4) and hence a trade-off between CO conversion, $CO_2$ capture efficiency and purity and solids elutriation should be made when selecting the optimum value of FR flowrate.

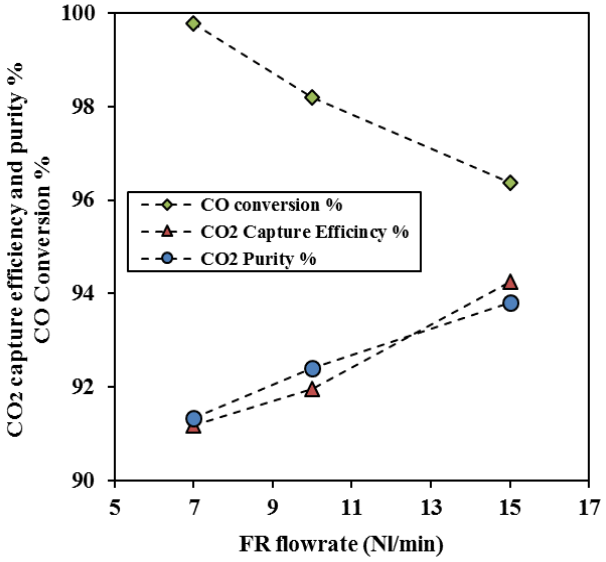


Fig. 12. $CO_2$ capture efficiency and purity and CO conversion with various FR flowrates, at AR flowrate = 50 Nl/min and a solids inventory = 1.5 kg (cases 1, 5 and 6).

### 3.3. Autothermal CLC operation in ICR

All the experience gained in the parametric study was used for designing an autothermal operation of the ICR without any external heat supply, where all the heat duties of the system are fulfilled by the heat generated in the CLC process. The energy balance over the autothermal ICR system is dominated by heat generation from fuel combustion, heat removal by the gases being heated up in the system, and heat losses from the reactor (which are generally large in lab-scale units). A high degree of fuel conversion is required to maximize heat generation from fuel combustion and the air flowrate can be adjusted to determine the reactor temperature under autothermal operation, with lower air flowrates resulting in higher temperatures.

Feeding 10 Nl/min of CO to the FR and 60 Nl/min of air in the AR using 1.5 kg solids inventory was found to achieve autothermal operation at a similar temperature to the other experiments conducted in the study. As can be seen in Fig. 13. stable temperatures were achieved in different measurement locations of the reactor without any external heating. Remarkably, the temperature at the bottom of the FR was higher than that in the AR despite the highly exothermic oxidation reaction taking place in the latter. This can be explained by the six times larger cold air feed to the AR than CO feed in the FR, in addition to the dilute solids flow nature in the AR chamber resulting in spatially distributed heat generation, in contrast to the concentrated heat generation in the FR due the dense solids flow (the employed OC has an exothermic reduction reaction with CO).

CO conversion was however only 97% (Case 7 in Table 4). To investigate the cause of CO slip, an additional experiment was conducted by increasing the AR flowrate to 70 Nl/min while keeping the same fuel input (case-8). Despite the increased solids circulation rate for 70 Nl/min (Table 4), CO conversion remained unchanged, which indicates that CO slip was due to the short-bed height in FR and not because of limitations in the solids circulation rate. Full conversion should be easily achievable in a larger-scale reactor with greater gas residence time.

Nevertheless, the ease and stability of ICR autothermal operation makes this configuration a prime candidate for replacing the interconnected fluidized bed reactor configuration for highly efficient chemical looping technology. However, the full potential of ICR configuration would only be proven if it demonstrates the ability of achieving acceptable levels of leakage between the ICR chambers at high pressure operation relevant to the foreseen industrial chemical looping conditions. This will be the scope of a future study.

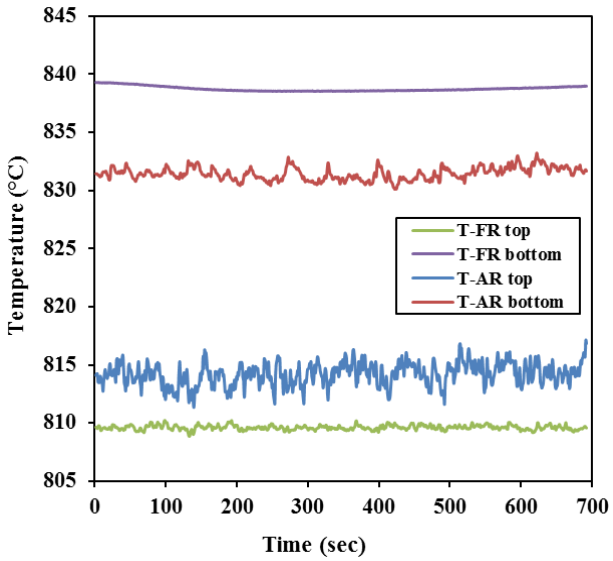


Fig. 13. Temperature profile in FR and AR during autothermal CLC test, AR flowrate = 60 Nl/min, FR flowrate = 10 Nl/min, solids inventory = 1.5 kg (case-7).

## 4. Summary and Conclusion

The present work presents a detailed study of the operating behavior of the internally circulating reactor (ICR) applied to chemical looping combustion (CLC). ICR is a promising reactor concept that aims to simplify the design and operation of pressurized chemical looping processes by eliminating the need for cyclones, loop seals and long solids transport lines between interconnected fluidized bed reactors. Instead, a single reactor vessel is used with internal partitions to create different reaction chambers with simple interconnecting ports for oxygen carrier circulation.

Good oxygen carrier circulation is essential for successful CLC operation. The study found the expected trends of increased solids circulation with greater solids loadings and greater differences between the feed rates to the different ICR chambers. Overall, sufficient oxygen carrier circulation could easily be achieved over a wide range of operating conditions.

The primary trade-off for the simplicity offered by the ICR concept is the reduction in $CO_2$ capture and purity caused by undesired gas leakage through the connecting ports. Large gas leakage was observed for higher bed loadings, but good performance of up to 94% $CO_2$ capture

and purity was achieved at the lowest bed loading investigated. Due to the short bed height in the fuel reactor for this bed loading, fuel conversion was only 97% in some cases, but 100% fuel conversion will be easily achievable in an upscaled reactor with greater gas residence time.

Results also showed that the $CO_2$ separation performance can be improved substantially in future studies by optimizing the bottom port. In an optimized unit, this port will be smaller and longer to minimize gas leakage resulting from instantaneous pressure difference reversals caused by dynamic pressure fluctuations from fluidization in the air and fuel reactors. However, the port must still be large enough to allow for sufficient solids circulation.

In conclusion, the ICR concept could be a promising candidate for accelerating scale-up and commercialization of pressurized chemical looping technologies. The reactor proved relatively simple to control over a range of operating conditions and showed predictable solids circulation and fuel conversion behavior. An autothermal experimental run was completed to demonstrate this ease of operation. Future investigation of the ICR concept is therefore strongly recommended, particularly pressurized demonstration and reactor scale-up studies with more optimized design.

## Acknowledgment

The authors would like to acknowledge the financial support of the Research Council of Norway under the CLIMIT program (project number: 255462). The technical support from the thermal engineering laboratory, especially Mr. Martin Bustadmo and Mr. Paul Svendsen are highly appreciated.

## References

[1] IEA (International Energy Agency). World Energy Outlook, Paris; 2018.

[2] J. Li, H. Zhang, Z. Gao, J. Fu, W. Ao, J. Dai, CO2 Capture with Chemical Looping Combustion of Gaseous Fuels: An Overview, Energy & Fuels. 31 (2017) 3475–3524.

[3] A. Lyngfelt, B. Leckner, T. Mattisson, A fluidized-bed combustion process with inherent CO2

separation; application of chemical-looping combustion, Chem. Eng. Sci. 56 (2001) 3101–3113.

[4] M.M. Hossain, H.I. De Lasa, Chemical-looping combustion (CLC) for inherent CO2 separations-a review, Chem. Eng. Sci. 63 (2008) 4433–4451.

[5] H.M. Kvamsdal, K. Jordal, O. Bolland, A quantitative comparison of gas turbine cycles with CO 2 capture, Energy. 32 (2007) 10–24.

[6] J. Wolf, M. Anheden, J. Yan, Comparison of nickel- and iron-based oxygen carriers in chemical looping combustion for CO capture in power generation, Fuel. 84 (2005) 993–1006.

[7] M. Rydén, A. Lyngfelt, Using steam reforming to produce hydrogen with carbon dioxide capture by chemical-looping combustion, Int. J. Hydrogen Energy. 31 (2006) 1271–1283.

[8] M. Ryden, A. Lyngfelt, T. Mattisson, Synthesis gas generation by chemical-looping reforming in a continuously operating laboratory reactor, Fuel. 85 (2006) 1631–1641.

[9] L.F. De Diego, M. Ortiz, F. García-Labiano, J. Adánez, A. Abad, P. Gayán, Hydrogen production by chemical-looping reforming in a circulating fluidized bed reactor using Ni-based oxygen carriers, J. Power Sources. 192 (2009) 27–34.

[10] T. Pröll, J. Bolhàr-Nordenkampf, P. Kolbitsch, H. Hofbauer, Syngas and a separate nitrogen/argon stream via chemical looping reforming – A 140 kW pilot plant study, Fuel. 89 (2010) 1249–1256.

[11] P. Ohlemüller, M. Reitz, J. Ströhle, B. Epple, Investigation of chemical looping combustion of natural gas at 1 MWth scale, Proc. Combust. Inst. 37 (2019) 4353–4360.

[12] A. Zaabout, S. Cloete, S.T. Johansen, M. Van, S. Annaland, F. Gallucci, S. Amini, Experimental Demonstration of a Novel Gas Switching Combustion Reactor for Power Production with Integrated CO2 Capture, Ind. Eng. Chem. Res. 52 (2013) 14241−14250.

[13] A. Zaabout, P.I. Dahl, A. Ugwu, J.R. Tolchard, S. Cloete, S. Amini, Gas Switching Reforming (GSR) for syngas production with integrated CO2 capture using iron-based oxygen carriers, Int. J. Greenh. Gas Control. 81 (2019) 170–180.

[14] A. Tong, L. Zeng, M. V. Kathe, D. Sridhar, L.-S. Fan, Application of the Moving-Bed Chemical Looping Process for High Methane Conversion, Energy & Fuels. 27 (2013) 4119–4128.

[15] T.-L. Hsieh, D. Xu, Y. Zhang, S. Nadgouda, D. Wang, C. Chung, Y. Pottimurphy, M. Guo, Y.-Y. Chen, M. Xu, P. He, L.-S. Fan, A. Tong, 250 kWth high pressure pilot demonstration of the syngas chemical looping system for high purity H2 production with CO2 capture, Appl. Energy. 230 (2018) 1660–1672.

[16] S.F. Håkonsen, R. Blom, Chemical Looping Combustion in a Rotating Bed Reactor – Finding Optimal Process Conditions for Prototype Reactor, Environ. Sci. Technol. 45 (2011) 9619–9626.

[17] C.O. Iloeje, Z. Zhao, A.F. Ghoniem, Design and techno-economic optimization of a rotary chemical looping combustion power plant with CO2 capture, Appl. Energy. 231 (2018) 1179–1190.

[18] A. Zaabout, S. Cloete, S. Amini, Innovative Internally Circulating Reactor Concept for Chemical Looping-Based CO2 Capture Processes: Hydrodynamic Investigation, Chem. Eng. Technol. 39 (2016) 1413–1424.

[19] M. Osman, A. Zaabout, S. Cloete, S. Amini, Internally circulating fluidized-bed reactor for syngas production using chemical looping reforming, Chem. Eng. J. (2018).

[20] S. Cloete, A. Zaabout, S. Amini, The Internally Circulating Reactor (ICR) Concept Applied to Pressurized Chemical Looping Processes, Energy Procedia. 114 (2017) 446–457.

[21] A. Zaabout, S. Cloete, J.R. Tolchard, S. Amini, A pressurized Gas Switching Combustion reactor: Autothermal operation with a CaMnO3−δ-based oxygen carrier, Chem. Eng. Res. Des. 137 (2018) 20–32.

[22] P. Hallberg, M. Hanning, M. Rydén, T. Mattisson, A. Lyngfelt, Investigation of a calcium manganite as oxygen carrier during 99 h of operation of chemical-looping combustion in a 10 kW th reactor unit, Int. J. Greenh. Gas Control. 53 (2016) 222–229.

[23] E. Bakken, T. Norby, S. Stølen, Nonstoichiometry and reductive decomposition of CaMnO3−δ, Solid State Ionics. 176 (2005) 217–223.

[24] H. Leion, Y. Larring, E. Bakken, R. Bredesen, T. Mattisson, A. Lyngfelt, Use of CaMn0.875Ti0.125O3 as Oxygen Carrier in Chemical-Looping with Oxygen Uncoupling, (2009).

[25] M. Arjmand, H. Leion, T. Mattisson, A. Lyngfelt, Investigation of different manganese ores as oxygen carriers in chemical-looping combustion (CLC) for solid fuels, Appl. Energy. 113 (2014) 1883–1894.

[26] A. Thon, M. Kramp, E.-U. Hartge, S. Heinrich, J. Werther, Operational experience with a system of coupled fluidized beds for chemical looping combustion of solid fuels using ilmenite as oxygen carrier, Appl. Energy. 118 (2014) 309–317.

[27] M. Rydén, A. Lyngfelt, T. Mattisson, CaMn 0.875 Ti 0.125 O 3 as oxygen carrier for chemical-looping combustion with oxygen uncoupling (CLOU)-Experiments in a continuously operating fluidized-bed reactor system, Int. J. Greenh. Gas Control. 5 (2010) 356–366.

[28] M. Rydén, M. Johansson, A. Lyngfelt, T. Mattisson, NiO supported on Mg–ZrO2 as oxygen carrier for chemical-looping combustion and chemical-looping reforming, Energy Environ. Sci. 2 (2009) 970.

[29] A. Abad, J. Adánez, F. García-Labiano, L.F. de Diego, P. Gayán, J. Celaya, Mapping of the range of operational conditions for Cu-, Fe-, and Ni-based oxygen carriers in chemical-looping combustion, Chem. Eng. Sci. 62 (2007) 533–549.

[30] M. Rydén, A. Lyngfelt, T. Mattisson, Chemical-looping combustion and chemical-looping reforming in a circulating fluidized-bed reactor using Ni-based oxygen carriers, Energy and Fuels. 22 (2008) 2585–2597.

[31] A. Abad, T. Mattisson, A. Lyngfelt, M. Ryden, Chemical-looping combustion in a 300W continuously operating reactor system using a manganese-based oxygen carrier, Fuel. 85 (2006) 1174–1185.

[32] M. Arjmand, M. Keller, H. Leion, T. Mattisson, A. Lyngfelt, Oxygen Release and Oxidation Rates of MgAl 2 O 4 -Supported CuO Oxygen Carrier for Chemical-Looping Combustion with Oxygen Uncoupling (CLOU), Energy & Fuels. 26 (2012) 6528–6539.

[33] Ajmal Latif, A study of the design of fluidized bed reactors for biomass gasification, PhD thesis. 1999.

[34] S. Shrestha, B.S. Ali, B.M. Jan, M.D.B. Hamid, K. El Sheikh, Hydrodynamic characteristics in cold model of dual fluidized bed gasifiers, Powder Technol. 286 (2015) 246–256.

[35] J.H. Goo, M.W. Seo, D. Kyoo Park, S.D. Kim, S.H. Lee, J.G. Lee, B.H. Song, Hydrodynamic Properties in a Cold-Model Dual Fluidized-Bed Gasifier, J. Chem. Eng. Japan. 41 (2008) 686–690.

[36] B. Kronberger, A. Lyngfelt, G. Löffler, H. Hofbauer, Design and Fluid Dynamic Analysis of a Bench-Scale Combustion System with CO 2 Separation−Chemical-Looping Combustion, Ind. Eng. Chem. Res. 44 (2005) 546–556.

[37] F.F. Snieders, A.C. Hoffmann, D. Cheesman, J.G. Yates, M. Stein, J.P.K. Seville, The dynamics of large particles in a four-compartment interconnected fluidized bed, Powder Technol. 101 (1999) 229–239.